

Nature of magnetic excitations in superconducting $\text{BaFe}_{1.9}\text{Ni}_{0.1}\text{As}_2$

Mengshu Liu¹, Leland W. Harriger¹, Huiqian Luo², Meng Wang^{1,2}, R. A. Ewings³, T. Guidi³, Hyowon Park⁴, Kristjan Haule⁴, Gabriel Kotliar⁴, S. M. Hayden⁵ and Pengcheng Dai^{1,2*}

Since the discovery of the metallic antiferromagnetic (AF) ground state near superconductivity in iron pnictide superconductors^{1–3}, a central question has been whether magnetism in these materials arises from weakly correlated electrons^{4,5}, as in the case of spin density wave in pure chromium⁶, requires strong electron correlations⁷, or can even be described in terms of localized electrons^{8,9} such as the AF insulating state of copper oxides¹⁰. Here we use inelastic neutron scattering to determine the absolute intensity of the magnetic excitations throughout the Brillouin zone in electron-doped superconducting $\text{BaFe}_{1.9}\text{Ni}_{0.1}\text{As}_2$ ($T_c = 20$ K), which allows us to obtain the size of the fluctuating magnetic moment $\langle m^2 \rangle$, and its energy distribution^{11,12}. We find that superconducting $\text{BaFe}_{1.9}\text{Ni}_{0.1}\text{As}_2$ and AF BaFe_2As_2 (ref. 13) both have fluctuating magnetic moments $\langle m^2 \rangle \approx 3.2 \mu_B^2$ per Fe(Ni), which are similar to those found in the AF insulating copper oxides^{14,15}. The common theme in both classes of high-temperature superconductors is that magnetic excitations have partly localized character, thus showing the importance of strong correlations for high-temperature superconductivity¹⁶.

In the undoped state, iron pnictides such as BaFe_2As_2 form a metallic low-temperature orthorhombic phase with the antiferromagnetic (AF) structure as shown in Fig. 1a (ref. 17). Inelastic neutron scattering measurements have mapped out spin waves throughout the Brillouin zone in the AF orthorhombic and paramagnetic tetragonal phases¹³. On Co- and Ni-doping to induce optimal superconductivity via electron doping, the orthorhombic structural distortion and static AF order in BaFe_2As_2 are suppressed and the system becomes tetragonal and paramagnetic at all temperatures¹⁸. In previous inelastic neutron scattering experiments on optimally electron-doped $\text{Ba}(\text{Fe}, \text{Co}, \text{Ni})_2\text{As}_2$ superconductors^{11,12,19–22}, spin excitations up to ~ 120 meV were observed. However, the lack of spin excitation data at higher energies in absolute units precluded a comparison with spin waves in undoped BaFe_2As_2 . Only the absolute intensity measurements in the entire Brillouin zone can reveal the effect of electron doping on the overall spin excitation spectra and allow a direct comparison with the results in the AF insulating copper oxides^{14,15}. For the experiments, we chose to study well-characterized electron-doped $\text{BaFe}_{1.9}\text{Ni}_{0.1}\text{As}_2$ (refs 20,22) because large single crystals were available²³ and their properties are similar to Co-doped BaFe_2As_2 (refs 11,12,19,21,24).

By comparing spin excitations in $\text{BaFe}_{1.9}\text{Ni}_{0.1}\text{As}_2$ and BaFe_2As_2 throughout the Brillouin zone, we were able to probe how electron doping and superconductivity affect the overall spin

excitation spectra. We demonstrate that whereas the low-energy spin excitations are affected, the high-energy excitations show a very weak temperature and doping dependence. Comparison of our results with various theories suggests that neither a fully itinerant nor a localized picture explains the magnetic excitation spectrum. However, a combination of density functional theory (DFT) and dynamic mean field theory (DMFT) provides a natural way to improve on both these pictures.

Figure 1c–e summarizes our key findings for the electron-doped iron arsenide superconductor $\text{BaFe}_{1.9}\text{Ni}_{0.1}\text{As}_2$ and the comparison with the spin waves in BaFe_2As_2 . The data points in Fig. 1c and d show the dispersion of spin excitations for optimally doped $\text{BaFe}_{1.9}\text{Ni}_{0.1}\text{As}_2$ along $[1, K]$ and $[H, 0]$ and the solid lines show the fit of BaFe_2As_2 spin waves to an effective Heisenberg $J_{1a} - J_{1b} - J_2$ model with $J_{1a} \neq J_{1b}$ (ref. 13). Figure 1e shows the local dynamic susceptibility per formula unit (*f.u.*), which contains two Fe(Ni) atoms, in absolute units, defined as $\chi''(\omega) = \int \chi''(\mathbf{q}, \omega) d\mathbf{q} / \int d\mathbf{q}$ (ref. 12), where $\chi''(\mathbf{q}, \omega) = (1/3) \text{tr}(\chi''_{\alpha\beta}(\mathbf{q}, \omega))$, at different energies for BaFe_2As_2 and $\text{BaFe}_{1.9}\text{Ni}_{0.1}\text{As}_2$. It is clear that electron doping on BaFe_2As_2 affects only the low-energy spin excitations by broadening the spin waves below 80 meV, but has no impact on spin waves above 100 meV (see Supplementary Information). The quasiparticles that form within the spin density wave gap are sensitive to the Fermi surface change on doping BaFe_2As_2 and, hence, the resulting low-energy itinerant spin excitations change substantially, whereas the higher energy spin excitations are hardly affected.

To substantiate the key conclusions from the data and calculations presented in Fig. 1, we show in Fig. 2 the two-dimensional constant-energy (*E*) images of spin excitations of $\text{BaFe}_{1.9}\text{Ni}_{0.1}\text{As}_2$ in the (H, K) scattering plane for several Brillouin zones at 5 K. In the undoped phase, spin waves in BaFe_2As_2 exhibit an anisotropy spin gap of $\Delta = 9.8$ meV (ref. 25). On doping, the anisotropy spin gap disappears and the spin excitations form transversely elongated ellipses that decrease in intensity with increasing energy^{12,21}. For energy transfers of $E = 10 \pm 3$, 33 ± 3 , 43 ± 3 , 60 ± 10 and 81 ± 10 meV (Fig. 2a–e), spin excitations are peaked at the AF wave vector $Q = (1, 0)$ in the centre of the Brillouin zone (shown as a dashed square box). As the energy increases to $E = 113 \pm 10$ and 135 ± 10 meV (Fig. 2f,g), spin excitations start to split along the K-direction and form a ring around the Γ point. Finally, spin excitations near the zone boundary at $E = 157 \pm 10$ and 214 ± 10 meV form four blobs centred at $Q = (1, 1)$ (Fig. 2h,i).

To determine the dispersion of spin excitations for $\text{BaFe}_{1.9}\text{Ni}_{0.1}\text{As}_2$, we cut through the two-dimensional images similar to Fig. 2 along the $[1, K]$ and $[H, 0]$ directions. Figure 3a–f shows

¹Department of Physics and Astronomy, The University of Tennessee, Knoxville, Tennessee 37996-1200, USA, ²Beijing National Laboratory for Condensed Matter Physics, Institute of Physics, Chinese Academy of Sciences, Beijing 100190, China, ³ISIS Facility, Rutherford Appleton Laboratory, Chilton, Didcot, Oxfordshire OX11 0QX, UK, ⁴Department of Physics, Rutgers University, Piscataway, New Jersey 08854, USA, ⁵H. H. Wills Physics Laboratory, University of Bristol, Tyndall Avenue, Bristol BS8 1TL, UK. *e-mail: pdai@utk.edu.

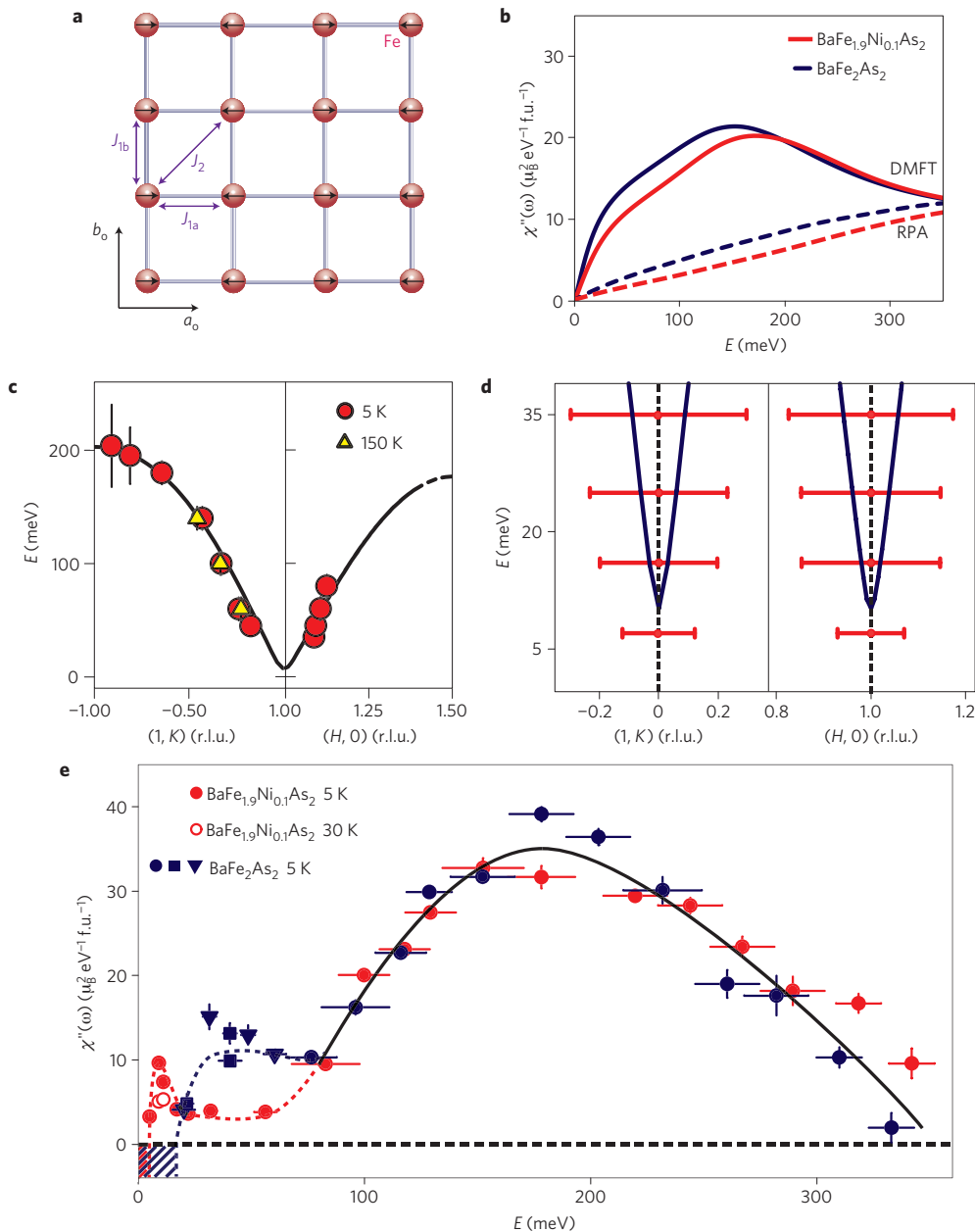


Figure 1 | Summary of neutron scattering and calculation results. Our experiments were carried out on the MERLIN time-of-flight chopper spectrometer at the Rutherford-Appleton Laboratory, UK (ref. 33). We co-aligned 28 g of single crystals of BaFe_{1.9}Ni_{0.1}As₂ (with in-plane mosaic of 2.5° and out-of-plane mosaic of 4°). The incident beam energies were $E_i = 20, 25, 30, 80, 250, 450, 600$ meV, and mostly with E_i parallel to the c axis. To facilitate easy comparison with spin waves in BaFe₂As₂ (ref. 13), we defined the wave vector Q at (q_x, q_y, q_z) as $(H, K, L) = (q_x a / 2\pi, q_y b / 2\pi, q_z c / 2\pi)$ reciprocal lattice units (r.l.u.) using the orthorhombic unit cell, where $a = b = 5.564$ Å, and $c = 12.77$ Å. The data are normalized to absolute units using a vanadium standard¹³, which may have a systematic error up to 20% owing to differences in neutron illumination of the vanadium and sample, and time-of-flight instruments. **a**, AF spin structure of BaFe₂As₂ with Fe spin ordering. The effective magnetic exchange couplings along different directions are shown. **b**, RPA and LDA+DMFT calculations of $\chi''(\omega)$ in absolute units for BaFe₂As₂ and BaFe_{1.9}Ni_{0.1}As₂. **c**, The solid lines show the spin wave dispersions of BaFe₂As₂ for $J_{1a} \neq J_{1b}$, along the $[1, K]$ and $[H, 0]$ directions obtained in ref. 13. The filled circles and triangles are the spin excitation dispersions of BaFe_{1.9}Ni_{0.1}As₂ at 5 K and 150 K, respectively. **d**, The solid line shows the low-energy spin waves of BaFe₂As₂. The horizontal bars show the full-width at half-maximum of spin excitations in BaFe_{1.9}Ni_{0.1}As₂. **e**, Energy dependence of $\chi''(\omega)$ for BaFe₂As₂ (filled blue circles) and BaFe_{1.9}Ni_{0.1}As₂ below (filled red circles) and above (open red circles) T_c . The solid and dashed lines are guides to the eye. The vertical error bars indicate statistical errors of one standard deviation. The horizontal error bars in **e** indicate the energy integration range.

constant-energy cuts along the $[1, K]$ direction for $E = 25 \pm 5, 55 \pm 5, 95 \pm 10, 125 \pm 10, 150 \pm 10,$ and 210 ± 10 meV. The scattering becomes dispersive for spin excitation energies above 95 meV. Figure 3g–i shows similar constant-energy cuts along the $[H, 0]$ direction. The solid lines in the figure show identical spin wave cuts for BaFe₂As₂ (ref. 13). As both measurements were taken in

absolute units, we can compare the impact of electron doping on the spin waves in BaFe₂As₂. At $E = 25 \pm 5$ meV, spin excitations in superconducting BaFe_{1.9}Ni_{0.1}As₂ are considerably broader in momentum space and weaker in intensity than spin waves (Fig. 3a,g). On increasing the excitation energy to 55 ± 5 meV, the dispersive spin waves in BaFe₂As₂ become weaker and broader (Fig. 3b,h).

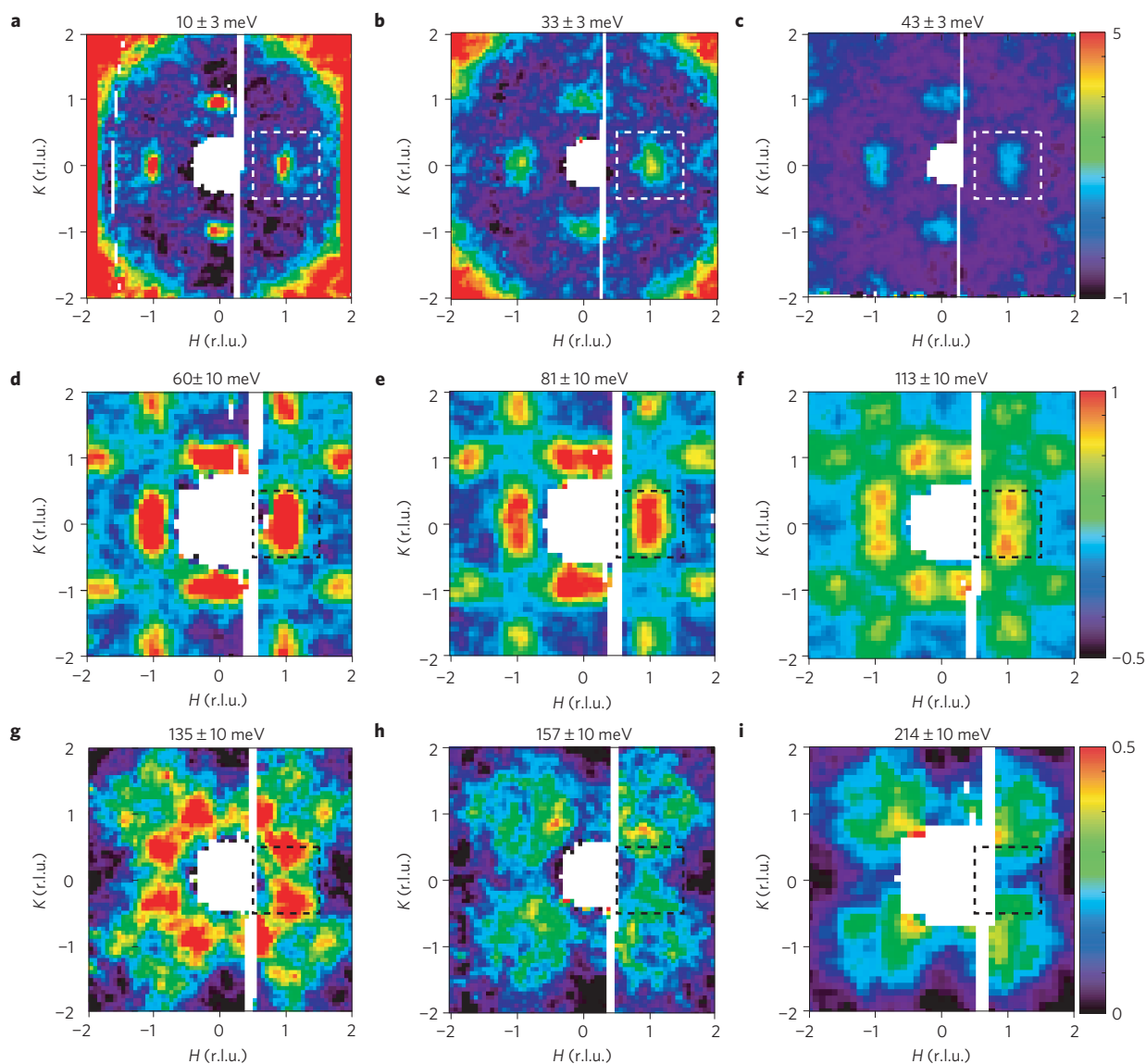


Figure 2 | Constant-energy slices through the magnetic excitations of $\text{BaFe}_{1.9}\text{Ni}_{0.1}\text{As}_2$ at different energies in several Brillouin zones. Two-dimensional images of spin excitations at the energies indicated. The images were obtained after subtracting the background integrated from $1.8 < H < 2.2$ and $-0.2 < K < 0.2$. The colour bars represent the vanadium-normalized absolute spin excitation intensity in the units of $\text{mb sr}^{-1} \text{meV}^{-1} \text{f.u.}^{-1}$ (mb is millibarn) and the dashed boxes indicate the AF zone boundaries for a single FeAs layer.

For energies above 95 meV, spin excitations in $\text{BaFe}_{1.9}\text{Ni}_{0.1}\text{As}_2$ are almost indistinguishable from spin waves in BaFe_2As_2 in both the linewidth and intensity (Fig. 3c–f,i). Based on these constant-energy cuts, we show in Fig. 1c,d the comparison of spin excitation dispersions of $\text{BaFe}_{1.9}\text{Ni}_{0.1}\text{As}_2$ (filled circles and horizontal bars) with those of spin waves in BaFe_2As_2 (solid lines). Inspection of Figs 1–3 reveals that electron doping to BaFe_2As_2 broadens and suppresses only low-energy spin excitations and has no influence on spin waves above 100 meV (see Supplementary Information).

To demonstrate further the effect of electron doping on the spin waves of BaFe_2As_2 , we show in Fig. 4a–d constant-Q cuts at different wave vectors along the $[1, K]$ direction for spin excitations in $\text{BaFe}_{1.9}\text{Ni}_{0.1}\text{As}_2$. Near the Brillouin zone centre at $Q = (1, 0.05)$ and $(1, 0.2)$, well-defined spin excitations are observed near $E = 40$ and 60 meV, as shown in Fig. 4a and b, respectively. The intensity of the scattering from the spin excitations in $\text{BaFe}_{1.9}\text{Ni}_{0.1}\text{As}_2$ is, however, much lower than that of BaFe_2As_2 , shown as solid lines in the figures. On increasing the wave vectors to $Q = (1, 0.35)$ and $(1, 0.5)$, the magnetic scattering peak near $E = 100$, and 120 meV,

and are essentially indistinguishable from spin waves in BaFe_2As_2 as shown in Fig. 4c and d. Furthermore, spin excitations have virtually no temperature dependence between 5 K and 150 K (Fig. 4b).

Finally, in Fig. 4e,f, we show the temperature dependence of spin excitations at energies near the neutron spin resonance $E = 9$ meV (refs 20,22) and at $E = 90 \pm 5$ meV, respectively. Whereas the intensity of the resonance at $E = 9$ meV increases markedly below T_c , consistent with earlier work^{20,22}, spin excitations at 90 ± 5 meV are identical on cooling from 150 K to 5 K. We note that high-energy spin waves in BaFe_2As_2 are also weakly temperature dependent¹³. Figure 4g shows the energy dependence of the dynamic spin–spin correlation lengths, which are about $\xi \approx 14$ Å and independent of excitation energy. For comparison, the dynamic spin–spin correlation length (the solid line in Fig. 4g) in BaFe_2As_2 decreases with increasing energy and becomes similar to that of $\text{BaFe}_{1.9}\text{Ni}_{0.1}\text{As}_2$ for excitation energies above 100 meV.

To check if spin excitations in the AF BaFe_2As_2 and superconducting $\text{BaFe}_{1.9}\text{Ni}_{0.1}\text{As}_2$ can be understood in an itinerant picture, we calculate the local susceptibility $\chi''(\omega)$ using the random

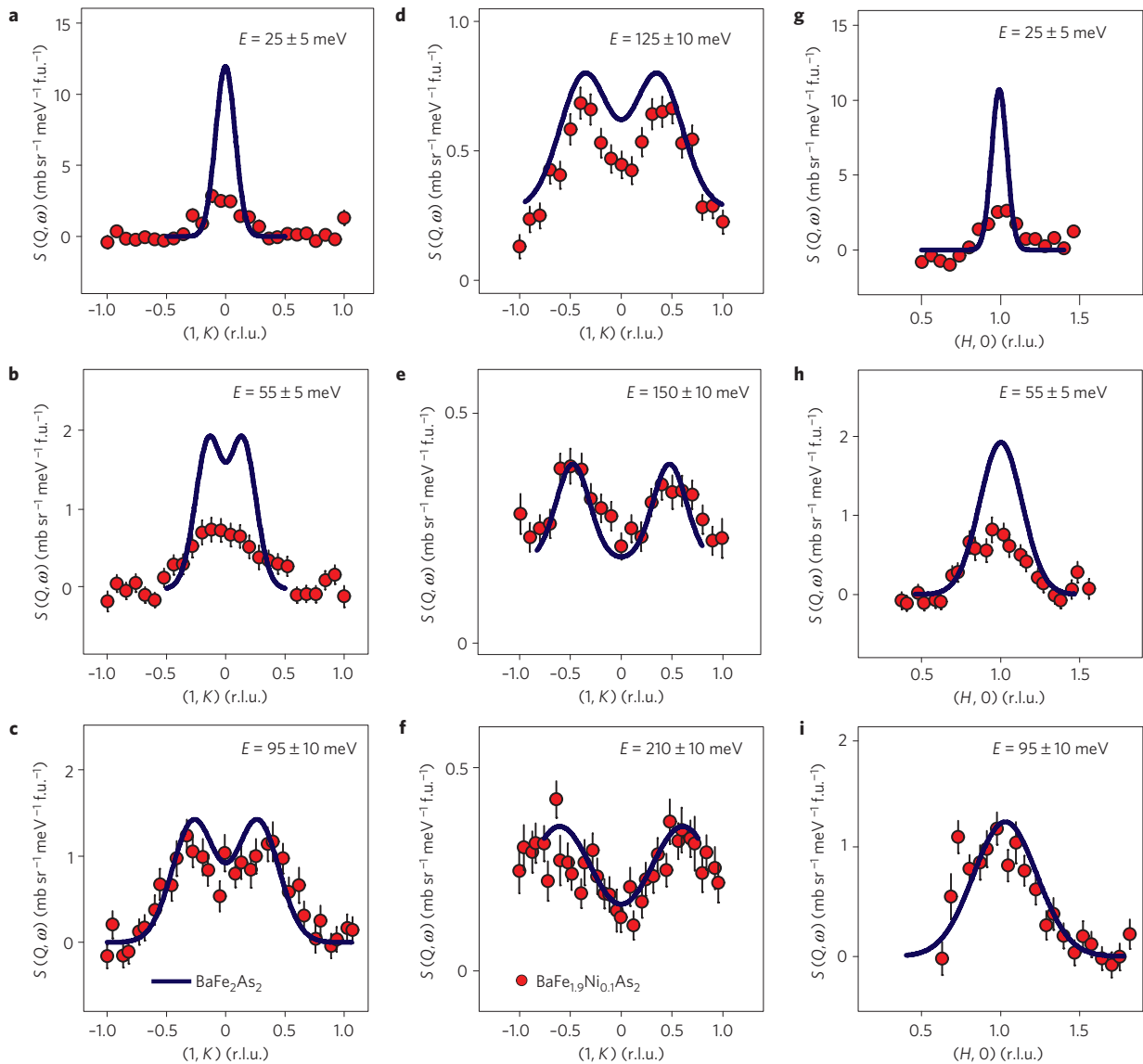


Figure 3 | Constant-energy cuts of the spin excitation dispersion as a function of increasing energy along the $[1, K]$ and $[H, 0]$ directions for $\text{BaFe}_{1.9}\text{Ni}_{0.1}\text{As}_2$. The solid lines show identical cuts for spin waves of BaFe_2As_2 in absolute units. **a–f**, Constant-energy cut along the $[1, K]$ direction at the energies indicated. **g–i** Constant-energy cut along the $[H, 0]$ direction at the energies indicated. The error bars indicate statistical errors of one standard deviation.

phase approximation (RPA) based on realistic Fermi surfaces and band structures²⁶. Within the RPA, the polarization bubble χ^0 is computed from the DFT using Kohn–Sham Green’s functions, while the irreducible vertex Γ^{irr} is approximated by the screened Coulomb parameters \tilde{U} and \tilde{J} . Using $\tilde{U} = 1.3$ eV and $\tilde{J} = 0.4$ eV and performing calculations above T_N (ref. 26), we find that the RPA estimate of $\chi''(\omega)$ for BaFe_2As_2 and $\text{BaFe}_{1.9}\text{Ni}_{0.1}\text{As}_2$ (dashed blue and red lines in Fig. 1b) increases approximately linearly with energy and has absolute values about a factor of three smaller than the observation (Fig. 1e). Although the RPA calculation depends on the Coulomb parameters used, we note that the five-orbital Hubbard model calculation using $\tilde{U} = 0.8$ eV and $\tilde{J} = 0.2$ eV produces essentially similar local magnetic spectra²⁷. Therefore, a pure RPA-type itinerant model underestimates the absolute spectral weight of the magnetic excitations in iron pnictides.

The solid blue and red lines in Fig. 1b show the calculated local susceptibility using a combined DFT and DMFT in the paramagnetic state. Within DFT + DMFT, $\chi''(\mathbf{q}, \omega)$ is computed by the Bethe–Salpeter equation using the polarization function χ^0 and the two-particle local irreducible vertex function Γ^{irr}

(ref. 26). χ^0 is computed from the interacting one-particle Green’s function determined by the charge self-consistent full potential DFT + DMFT method and Γ^{irr} is extracted from the two-particle vertex function of the auxiliary impurity problem. The latter is defined by the DMFT procedure using the projection of all electronic states to the d character within the iron muffin–tin sphere. By comparing DFT + DMFT and RPA calculations in Fig. 1b with data in Fig. 1e, we see that the former is much closer to the observation. Note that the calculation is done in the paramagnetic state, hence the low-energy modifications of the spectra due to the long range AF order are not captured in this calculation. RPA can describe only the itinerant part of the electron spectra, whereas DFT + DMFT captures the essential aspects of both the quasiparticles and the local moments of iron formed by strong Hund’s coupling (see Supplementary Information for a more detailed discussion). The improved agreement of DFT + DMFT thus suggests that both the quasiparticles and the local moment aspects of the electrons of iron are needed to obtain the correct intensity and energy distribution of neutron scattering spectra²⁶.

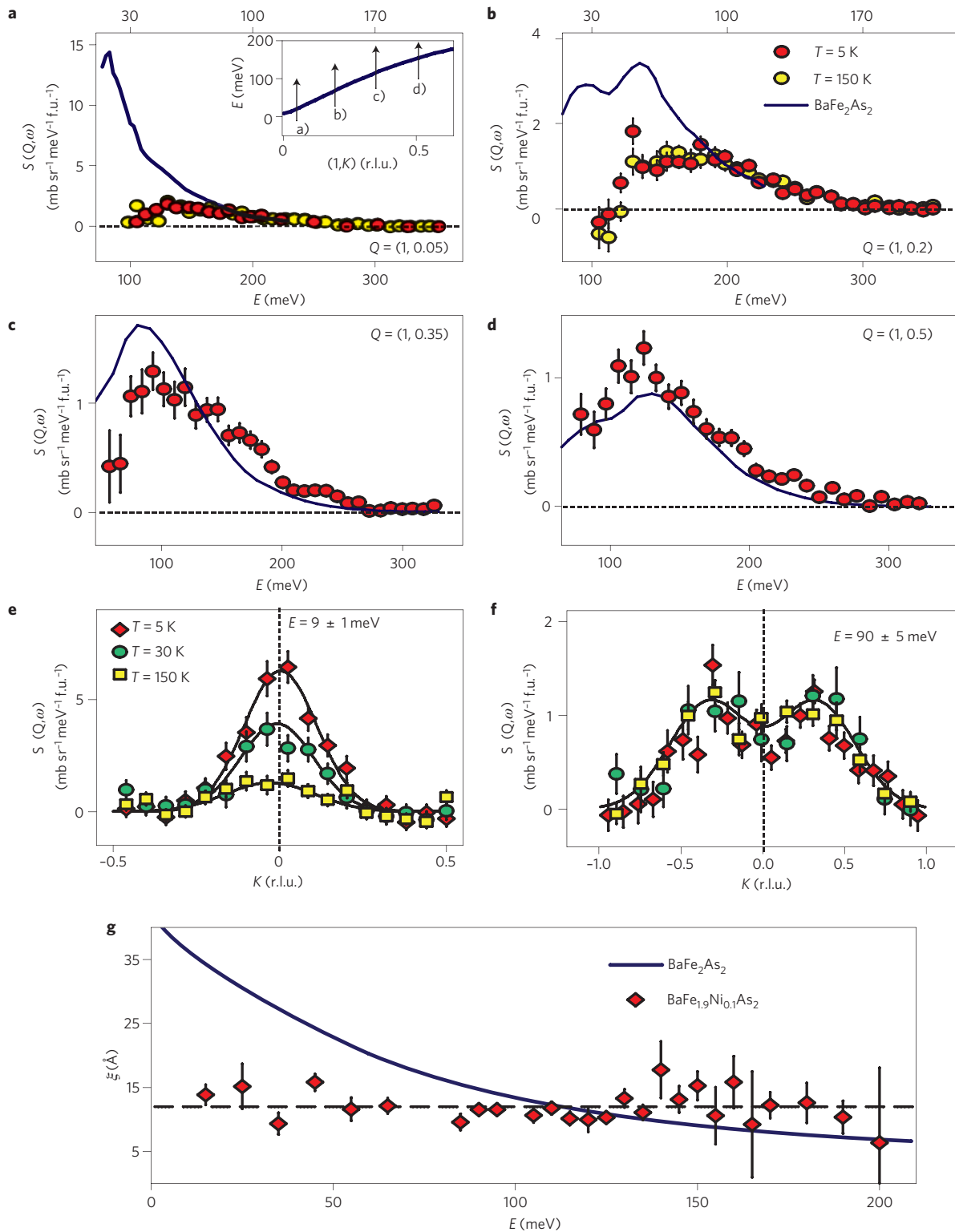


Figure 4 | Constant-energy/wave-vector (Q) dependence of the spin excitations and dynamic spin-spin correlation lengths for $\text{BaFe}_{1.9}\text{Ni}_{0.1}\text{As}_2$ and BaFe_2As_2 . **a–d**, Constant- Q cuts at $Q = (1, 0.05)$, $(1, 0.2)$, $(1, 0.35)$, and $(1, 0.5)$, respectively, at $T = 5$ (solid red circles) and 150 K (yellow filled circles), with the background at $Q = (2, 0)$ subtracted. The negative scattering in the data is due to oversubtraction of the phonon background. The solid lines are identical cuts from spin waves in BaFe_2As_2 . For excitations below 100 meV, the intensity of the scattering of $\text{BaFe}_{1.9}\text{Ni}_{0.1}\text{As}_2$ is suppressed compared with that of BaFe_2As_2 . For energies above 100 meV, the magnetic scattering is virtually identical between the parent and superconductor. Inset indicates the Q -cuts shown in **a–d**. **e**, Constant-energy cuts at the neutron spin resonance energy of $E = 9 \pm 1$ meV (ref. 20) below and above T_c . The solid lines are Gaussian fits on linear backgrounds. **f**, Temperature dependence of spin excitations at $E = 90 \pm 5$ meV. **g**, Energy dependence of the dynamic spin-spin correlation lengths (ξ) at 5 K obtained from a Fourier transform of constant-energy cuts similar to those in Fig. 3a–f and Fig. 4e,f. For all the excitation energies probed ($10 \leq E \leq 200$ meV), the dynamic spin-spin correlation lengths are independent of energy. The solid line shows the energy dependence of ξ for BaFe_2As_2 . The error bars indicate statistical errors of one standard deviation.

One way to quantitatively compare spin excitations in iron pnictides with those in copper oxides is to estimate their total fluctuating moments, defined as $\langle m^2 \rangle = (3\hbar/\pi) \int \chi''(\omega) d\omega / (1 - \exp(-\hbar\omega/kT))$ (ref. 12). Based on Fig. 1e, we find that $\langle m^2 \rangle = 3.17 \pm 0.16$ and $3.2 \pm 0.16 \mu_B^2$ per Fe(Ni) for BaFe_2As_2 and $\text{BaFe}_{1.9}\text{Ni}_{0.1}\text{As}_2$, respectively. Using the formula for magnetic moment of a spin $\langle m^2 \rangle = (g\mu_B)^2 S(S+1)$ (where $g = 2$; ref. 28), we find an effective iron spin S of about $1/2$, similar to that of CaFe_2As_2 (ref. 29). These results also show that superconductivity in electron-doped system hardly changes the total size of the fluctuating moment. In the fully localized (insulating) case, the formal Fe^{2+} oxidation state in BaFe_2As_2 would give a $3d^6$ electronic configuration. Hund's rules would yield $S = 2$ and $\langle m^2 \rangle = 24 \mu_B^2$ per Fe. This is considerable more than the observed values, suggesting significant hybridization of Fe $3d$ with pnictide p orbitals and among themselves, which leads to a metallic state where the Hund's coupling is less important than in the atomic limit³⁰. For comparison, we note that $\langle m^2 \rangle > 1.9 \mu_B^2$ per Cu for the AF insulating La_2CuO_4 measured over a similar energy range^{14,15}. From Fig. 1e, we see that the large fluctuating moment (m^2) in iron pnictides arises mostly from high-energy spin excitations that are essentially independent of temperature¹³ and electron doping within the errors of our measurements (Fig. 1). As there are currently no high-energy spin excitation data in absolute units for optimally hole-doped $\text{Ba}_{0.67}\text{K}_{0.33}\text{Fe}_2\text{As}_2$ (ref. 31), it is unclear how hole doping BaFe_2As_2 modifies the spin-wave spectra.

The DFT + DMFT calculation suggests that both the band structure and the local moment aspects (for example Hund's coupling) of the iron electrons are needed to obtain a good description of the magnetic response in BaFe_2As_2 and $\text{BaFe}_{1.9}\text{Ni}_{0.1}\text{As}_2$. The weak dependence of the fluctuating moment on electron doping is consistent with the Hund's metal picture, where electron filling associated with the Fe $3d^6$ electrons by Ni-doping is not expected to drastically affect the local moments. What is surprising is that the similarities between the local susceptibilities of the iron pnictides studied here and the parents of the cuprate superconductors. The large fluctuating moment, arising from Hund's rule coupling, and concentrated at higher energy in iron pnictides, nevertheless gives an imprint on the massive and anisotropic low-energy quasiparticles³², which form Cooper pairs at low energy. This physics is different from the physics of the doped charge transfer insulators appropriate for copper oxides¹⁰, hence the electron correlations in iron pnictides and copper oxides have different microscopic origins, although they are important for understanding the magnetism and superconductivity in both materials.

Received 8 July 2011; accepted 16 February 2012; published online 25 March 2012

References

- Kamihara, Y., Watanabe, T., Hirano, M. & Hosono, H. Iron-based layered superconductor $\text{La}[\text{O}_{1-x}\text{F}_x]\text{FeAs}$ ($x = 0.05\text{--}0.12$) with $T_c = 26$ K. *J. Am. Chem. Soc.* **130**, 3296–3297 (2008).
- De la Cruz, C. *et al.* Magnetic order close to superconductivity in the iron-based layered $\text{LaO}_{1-x}\text{F}_x\text{FeAs}$ systems. *Nature* **453**, 899–902 (2008).
- Paglione, J. & Greene, R. L. High-temperature superconductivity in iron-based materials. *Nature Phys.* **6**, 645–658 (2010).
- Mazin, I. I., Singh, D. J., Johannes, M. D. & Du, M. H. Unconventional superconductivity with a sign reversal in the order parameter of $\text{LaFeAsO}_{1-x}\text{F}_x$. *Phys. Rev. Lett.* **101**, 057003 (2008).
- Dong, J. *et al.* Competing orders and spin-density-wave instability in $\text{LaO}_{1-x}\text{F}_x\text{FeAs}$. *Europhys. Lett.* **83**, 27006 (2008).
- Fawcett, E. Spin-density-wave antiferromagnetism in chromium. *Rev. Mod. Phys.* **60**, 209–283 (1988).
- Haule, K., Shim, J. H. & Kotliar, G. Correlated electronic structure of $\text{LaO}_{1-x}\text{F}_x\text{FeAs}$. *Phys. Rev. Lett.* **100**, 226402 (2008).
- Si, Q. & Abrahams, E. Strong correlations and magnetic frustration in the high T_c iron pnictides. *Phys. Rev. Lett.* **101**, 076401 (2008).
- Xu, C. K., Müller, M. & Sachdev, S. Ising and spin orders in the iron-based superconductors. *Phys. Rev. B* **78**, 020501(R) (2008).
- Lee, P. A., Nagaosa, N. & Wen, X.-G. Doping a Mott insulator: Physics of high-temperature superconductivity. *Rev. Mod. Phys.* **78**, 17–85 (2006).
- Inosov, D. S. *et al.* Normal-state spin dynamics and temperature-dependent spin-resonance energy in optimally doped $\text{BaFe}_{1.85}\text{Co}_{0.15}\text{As}_2$. *Nature Phys.* **6**, 178–181 (2010).
- Lester, C. *et al.* Dispersive spin fluctuations in the nearly optimally doped superconductor $\text{Ba}(\text{Fe}_{1-x}\text{Co}_x)_2\text{As}_2$ ($x = 0.065$). *Phys. Rev. B* **81**, 064505 (2010).
- Harriger, L. W. *et al.* Nematic spin fluid in the tetragonal phase of BaFe_2As_2 . *Phys. Rev. B* **84**, 054544 (2011).
- Headings, N. S., Hayden, S. M., Coldea, R. & Perring, T. G. Anomalous high-energy spin excitations in the high- T_c superconductor-parent antiferromagnet La_2CuO_4 . *Phys. Rev. Lett.* **105**, 247001 (2010).
- Hayden, S. M. *et al.* Comparison of the high-frequency magnetic fluctuations in insulating and superconducting $\text{La}_{2-x}\text{Sr}_x\text{CuO}_4$. *Phys. Rev. Lett.* **76**, 1344–1347 (1996).
- Basov, D. N. & Chubukov, A. V. Manifesto for a higher T_c . *Nature Phys.* **7**, 272–276 (2011).
- Huang, Q. *et al.* Neutron-diffraction measurements of magnetic order and a structural transition in the parent BaFe_2As_2 compound of FeAs-based high-temperature superconductors. *Phys. Rev. Lett.* **101**, 257003 (2008).
- Lester, C. *et al.* Neutron scattering study of the interplay between structure and magnetism in $\text{Ba}(\text{Fe}_{1-x}\text{Co}_x)_2\text{As}_2$. *Phys. Rev. B* **79**, 144523 (2009).
- Lumsden, M. D. *et al.* Two-dimensional resonant magnetic excitation in $\text{BaFe}_{1.84}\text{Co}_{0.16}\text{As}_2$. *Phys. Rev. Lett.* **102**, 107005 (2009).
- Chi, S. *et al.* Inelastic neutron-scattering measurements of a three-dimensional spin resonance in the FeAs-based $\text{BaFe}_{1.9}\text{Ni}_{0.1}\text{As}_2$ superconductor. *Phys. Rev. Lett.* **102**, 107006 (2009).
- Li, H. F. *et al.* Anisotropic and quasipropagating spin excitations in superconducting $\text{Ba}(\text{Fe}_{0.926}\text{Co}_{0.074})_2\text{As}_2$. *Phys. Rev. B* **82**, 140503(R) (2010).
- Wang, M. Y. *et al.* Electron-doping evolution of the low-energy spin excitations in the iron arsenide superconductor $\text{BaFe}_{2-x}\text{Ni}_x\text{As}_2$. *Phys. Rev. B* **81**, 174524 (2010).
- Chen, Y. C., Lu, X. Y., Wang, M., Luo, H. Q. & Li, S. L. Systematic growth of $\text{BaFe}_{2-x}\text{Ni}_x\text{As}_2$ large crystals. *Supercond. Sci. Technol.* **24**, 065004 (2011).
- Bud'ko, S. L., Ni, N. & Canfield, P. C. Jump in specific heat at the superconducting transition temperature in $\text{Ba}(\text{Fe}_{1-x}\text{Co}_x)_2\text{As}_2$ and $\text{Ba}(\text{Fe}_{1-x}\text{Ni}_x)_2\text{As}_2$ single crystals. *Phys. Rev. B* **79**, 220516(R) (2009).
- Matan, K., Morinaga, R., Lida, K. & Sato, T. J. Anisotropic itinerant magnetism and spin fluctuations in BaFe_2As_2 : A neutron scattering study. *Phys. Rev. B* **79**, 054526 (2009).
- Park, H., Haule, K. & Kotliar, G. Magnetic excitation spectra in BaFe_2As_2 : A two-particle approach within a combination of the density functional theory and the dynamical mean-field theory method. *Phys. Rev. Lett.* **107**, 137007 (2011).
- Graser, S. *et al.* Spin fluctuations and superconductivity in a three-dimensional tight-binding model for BaFe_2As_2 . *Phys. Rev. B* **81**, 214503 (2010).
- Lorenzana, J., Seibold, G. & Coldea, R. Sum rules and missing spectral weight in magnetic neutron scattering in the cuprates. *Phys. Rev. B* **72**, 224511 (2005).
- Zhao, J. *et al.* Spin waves and magnetic exchange interactions in CaFe_2As_2 . *Nature Phys.* **5**, 555–560 (2009).
- Cvetkovic, V. & Tesanovic, Z. Multiband magnetism and superconductivity in Fe-based compounds. *Europhys. Lett.* **85**, 37002 (2009).
- Zhang, C. L. *et al.* Neutron Scattering Studies of spin excitations in hole-doped $\text{Ba}_{0.67}\text{K}_{0.33}\text{Fe}_2\text{As}_2$ superconductor. *Sci. Rep.* **1**, 115 (2011).
- Yin, Z. P., Haule, K. & Kotliar, G. Magnetism and charge dynamics in iron pnictides. *Nature Phys.* **7**, 294–297 (2011).
- Bewley, R. I. *et al.* MERLIN, a new high count rate spectrometer at ISIS. *Physica B* **385–386**, 1029–1031 (2006).

Acknowledgements

We thank T. A. Maier, J. P. Hu and T. Xiang for helpful discussions. The work at Knoxville is supported by the US National Science Foundation (NSF) DMR-1063866 and OISE-0968226. Work at the Institute of Physics is supported by the Ministry of Science and Technology China 973 programs (2012CB821400, 2011CBA00110) and National Natural Science Foundation of China (NSFC-11004233). The work at Rutgers is supported by Department of Energy (DOE) BES DE-FG02-99ER45761 (G.K.), American Chemical Society Petroleum Research Fund 48802 and the Alfred P. Sloan foundation (K.H.).

Author contributions

P.D. and M.L. planned neutron scattering experiments. M.L., L.W.H., H.L., R.A.E., T.G. and P.D. carried out neutron scattering experiments. Data analysis was done by M.L. with help from L.W.H., R.A.E., T.G. and S.M.H. The samples were grown by H.L. and co-aligned by M.L. and M.W. The DFT and DMFT calculations were done by H.P., K.H. and G.K. The paper was written by P.D., K.H. and G.K. with input from S.M.H. and M.L. All coauthors provided comments on the paper.

Additional information

The authors declare no competing financial interests. Supplementary information accompanies this paper on www.nature.com/naturephysics. Reprints and permissions information is available online at www.nature.com/reprints. Correspondence and requests for materials should be addressed to P.D.